NOVEMBER 08 2016

Reconstruction of piano hammer force from string velocity

Antoine Chaigne

J. Acoust. Soc. Am. 140, 3504–3517 (2016)
https://doi.org/10.1121/1.4965965

Reconstruction of piano hammer force from string velocity

Antoine Chaigne[a)]
Institute of Music Acoustics, University of Music and Performing Arts Vienna, Anton-von-Webern-Platz 1, 1030 Vienna, Austria

(Received 18 March 2016; revised 5 October 2016; accepted 10 October 2016; published online 8 November 2016)

A method is presented for reconstructing piano hammer forces through appropriate filtering of the measured string velocity. The filter design is based on the analysis of the pulses generated by the hammer blow and propagating along the string. In the five lowest octaves, the hammer force is reconstructed by considering two waves only: the incoming wave from the hammer and its first reflection at the front end. For the higher notes, four- or eight-wave schemes must be considered. The theory is validated on simulated string velocities by comparing imposed and reconstructed forces. The simulations are based on a nonlinear damped stiff string model previously developed by Chabassier, Chaigne, and Joly [J. Acoust. Soc. Am. **134**(1), 648–665 (2013)]. The influence of absorption, dispersion, and amplitude of the string waves on the quality of the reconstruction is discussed. Finally, the method is applied to real piano strings. The measured string velocity is compared to the simulated velocity excited by the reconstructed force, showing a high degree of accuracy. A number of simulations are compared to simulated strings excited by a force derived from measurements of mass and acceleration of the hammer head. One application to an historic piano is also presented.

[http://dx.doi.org/10.1121/1.4965965]

[TRM] Pages: 3504–3517

I. INTRODUCTION

In pianos, precise knowledge of the hammer force in terms of amplitude, duration, and shape is essential since it fully determines the resulting free vibrations of the strings. Therefore, it is not surprising that a vast literature exists on this matter in piano acoustics. For years, one commonly used method for deriving the force consisted in multiplying together the measured mass and acceleration of the hammer head.[1,2] This method yields an acceptable rough estimate of the hammer pulse, though it suffers from several limitations.[3] Among these limitations, the oscillations of the hammer shank were highlighted experimentally by several authors in the past,[4,5] and confirmed by recent simulations.[6] With the emergence of new optical techniques and, in particular, of those using high-speed cameras, new methods are now available for measuring the hammer force with great accuracy.[3]

In this paper, an alternative method is proposed for determining the hammer force. This method is based on non-contact measurements of the string velocity from which the hammer force is derived through appropriate filtering based on the properties of the wave propagation along the string. The underlying motivation of this method follows from the observation that the hammer is not always easily accessible on all pianos and, in addition, that sophisticated optical methods cannot always be simply implemented in all situations. This fact has been experienced by the author during experiments on historic pianofortes, for which conservation requirements impose to find fast, portable, and non-intrusive measurements. A similar approach was used in the past for the bowed string.[7]

The basic principles of the reconstruction method are presented in Sec. II for a linear undamped nondispersive string (a so-called "ideal" string) excited by an imposed hammer force pulse $f_H(t)$ of finite duration τ_H at a given striking position x_H. The transverse string velocity $v_s(t)$ is measured at a given position x_s along the string. The initial transient part of $v_s(t)$ is represented by the finite sum of elementary waves generated by the hammer, and traveling back and forth along the string. For piano strings, it is shown that 2 to 8 waves are sufficient for representing this initial transient adequately for the complete piano compass, the number of waves to be considered depending on both the fundamental frequency f_1 of the note and force width τ_H. A classical comb filter is applied to $v_s(t)$ in order to reconstruct the hammer force. The appropriate choice of x_s is imposed by the properties of the filter.

In Sec. III, the method is applied to simulated piano strings. The simulations are based on a model of a damped nonlinear stiff string recently developed by Chabassier *et al.*[8] The physical parameters of the simulated strings are measured on real pianos. The string is excited by an imposed hammer force pulse. This input force has realistic amplitude, time width, and shape for each simulated note. The pertinence of the wave filtering method is validated by comparisons between the input force and the reconstructed force. Three different types of wave filters are used in order to cover the complete range of notes of a piano keyboard. The influence of damping, stiffness, and amplitude of the string motion on the estimation of the hammer force are examined.

a)Electronic mail: antchaigne@gmail.com

In Sec. IV, the method is applied to measured piano strings. The string velocity is measured with a calibrated electromagnetic sensor. The reconstructed hammer force serves as the input force for the corresponding simulated string, and the resulting simulated velocity is compared to the measured velocity. In some particular cases, the reconstructed hammer force is compared to the force derived from measurements of hammer head acceleration and mass, and the influence of hammer shank motion is discussed. Finally, an example of application of the method to an historic piano with a Viennese action is presented.

II. THEORY

A. Ideal piano string model

In this section, it is assumed that the motion of the piano string is described by a linear wave equation without damping or stiffness terms. The string is characterized by its tension at rest T_0, length L, and linear mass density μ. The string is rigidly fixed at both ends, agraffe (A) and bridge (B), which are considered as perfectly reflecting boundaries. Only one transverse component of the string motion $y(x,t)$ is considered, in the direction of the initial hammer velocity, which is here assumed to be vertical. In this ideal case, the equations of the struck string are written[9,10]

$$\mu\frac{\partial^2 y}{\partial t^2} - T_0\frac{\partial^2 y}{\partial x^2} = f_H(t)\delta(x - x_H), \quad \forall x \in [0, L],$$
$$y(x = 0, t) = 0, \quad y(x = L, t) = 0, \qquad (1)$$

where $f_H(t)$ is a hammer force of finite duration τ_H applied at the striking position x_H, and δ is the Dirac delta function. The transverse speed is $c = \sqrt{T_0/\mu}$, the fundamental frequency is $f_1 = 1/T_1 = c/2L$, and $Z_c = \sqrt{\mu T_0}$ is the characteristic impedance.[9] In pianos, the striking point is situated at a distance roughly equal to $L/10$ from the agraffe.[11] The string velocity $v_s(t)$ is measured at position x_s. Figure 1 shows the case where x_s is situated between agraffe and hammer. Both situations $x_s < x_H$ and $x_s > x_H$ will be examined in this section. At position x_H, the hammer blow generates two pulses $v_{sh}(t) = f_H(t)/2Z_c$ traveling in opposite directions: the left wave toward the agraffe (A), and the right wave toward the bridge (B). These elementary pulses reach the sensor position at successive instants of time t_i whose expressions are given in the Appendix.

In Sec. II B, an intuitive analysis of the wave propagation on the string is presented, showing that the number of elementary pulses (or waves) to consider in the measured string velocity to reconstruct the hammer force depend on the ratio between the force width τ_H and the string period T_1. For pianos, this leads to the elaboration of two-, four- and eight-wave schemes, depending on the played note. In Sec. II C, it is shown that these three schemes are particular cases of a general formulation of the transfer function between string velocity and hammer force that needs to be inverted in order to recover the force. This inversion imposes precautions in the measurements and, in particular, in the appropriate selection of the measuring point x_s.

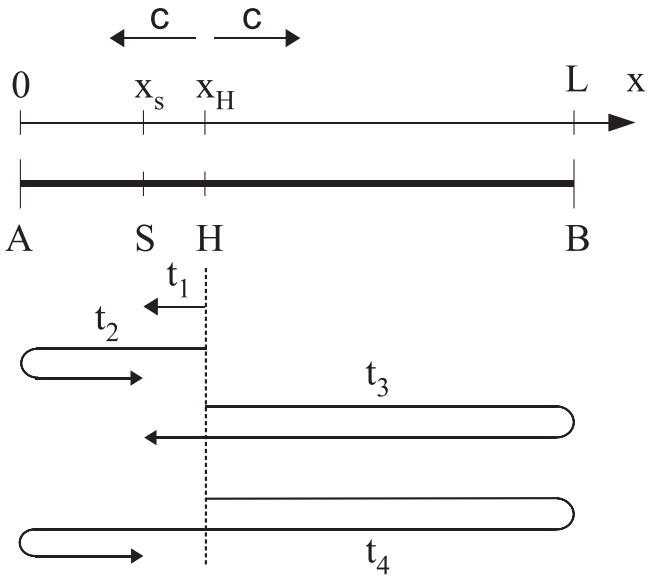

FIG. 1. Simplified geometry of a piano string with agraffe (A), speaking length L, bridge (B), measuring position x_s of the sensor (S), striking position x_H of the hammer (H), and traveling waves at speed c. Case $x_s < x_H$. The t_i are the successive instants of time where the pulses reach the sensor.

B. Principles of the force reconstruction method. Wave analysis

1. Bass and medium range of the piano. Two-wave scheme

Reconstructing the hammer force from the string velocity is an inverse problem. Knowing $v_s(t)$, the goal is to recover the force pulse $f_H(t)$ through the analysis of the wave propagation on the string and the reflection of the pulses at the boundaries (agraffe and bridge). Figure 2 illustrates this point in the typical case of a piano note in the bass (or medium) range, where the string velocity waveform recorded near the agraffe is clearly separated into two distinct parts. In the presented case where $x_s < x_H$, the first part of $v_s(t)$ is proportional to the sum of the incoming hammer

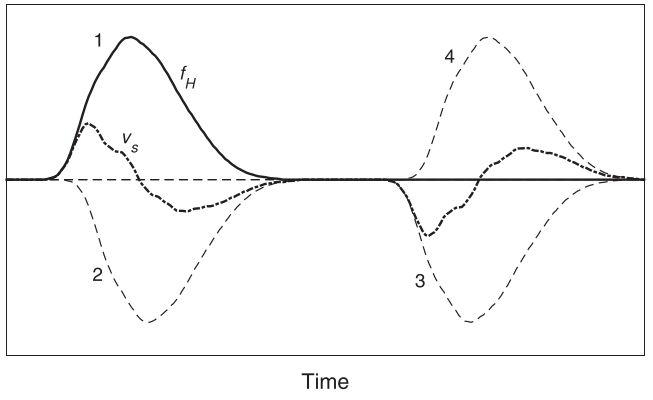

FIG. 2. Example of decomposition of the string velocity v_s (dashed-dotted line) measured at the sensor position in the situation $x_s < x_H$ shown in Fig. 1, when the width τ_H of the force pulse is small compared to the period (bass and medium range of the piano). The first part of the measured velocity is proportional to the sum of the first incoming force pulse (1: solid line) and of its reflection at the agraffe (2: dashed). The second part is proportional to the sum of the pulse reflected at the bridge (3: dashed) and of its reflection at the agraffe (4: dashed).

force pulse (1) and its reflection at the agraffe (2), whereas its second part is proportional to the sum of the force pulses reaching the sensor after reflection at the bridge (3) and after further reflection at the agraffe (4). Each reflection at either end is characterized by a change of sign. Using the notations defined in Sec. II A, we can write for the first part of $v_s(t)$,

$$v_s(t) = \frac{1}{2Z_c}\left[f_H\left(t - \frac{x_H - x_s}{c}\right) - f_H\left(t - \frac{x_H + x_s}{c}\right)\right]. \quad (2)$$

The calculation in the Appendix shows that Eq. (2) can be used to reconstruct the hammer force pulse as long as its width τ_H is such that

$$\tau_H < \frac{2(L - x_H)}{c} = \frac{L - x_H}{L}\, T_1. \quad (3)$$

This condition is obtained by considering that the force pulse (1) goes to zero before the third pulse reaches the sensor. In other words, Eq. (3) means that the number of elementary waves to consider for the reconstruction is equal to the number of waves reaching the sensor during the duration τ_H of the force pulse width. Since x_H usually is on the order of $L/10$, the condition in Eq. (3) corresponds to a force pulse duration slightly smaller than the period T_1 of the string's oscillation. In practice, Fig. 3 shows that this condition is fulfilled for most pianos below the note C5. In this range, the force reconstruction method then consists in inverting the two-wave scheme expressed in Eq. (2). This inversion is achieved by applying a dedicated so-called reconstruction filter to the string velocity, as explained in Sec. II C. Analysis of the filter properties will show why the velocity sensor must be placed near the agraffe for this two-wave scheme.

2. Upper range of the piano. Four- and eight-wave schemes

In pianos, the width of the force pulse decreases less rapidly than the period of the string's oscillation when moving toward the treble range (see Fig. 3). As a consequence, the propagating pulses get closer to one another and several reflections can occur during the pulse width τ_H. It is shown in the Appendix that, under the condition

$$2(L - x_H) < c\tau_H < 2L, \quad (4)$$

the initial force pulse goes to zero before the fifth reflected pulse reaches the sensor. Therefore, the string velocity can be represented by a sum of four waves during the initial time interval τ_H. An example is shown in Fig. 4. The frequency analysis of the corresponding reconstruction filter then shows that the measuring point of the string velocity x_s now must be close to the bridge in order to recover the force properly (see Sec. II C). In practice, the condition in Eq. (4) required for this four-wave scheme is rather restrictive. It is fulfilled in a small range of notes for most pianos, usually between the notes C5 and C6 (see Fig. 3).

For the remaining two upper octaves of the piano (notes C6–C8), a typical situation is shown in Fig. 5. In the example presented here, it is seen that the first six pulses are involved in the expression of $v_s(t)$ over the duration τ_H of the initial force pulse. Following the same reasoning as previously, we could think of considering six waves over this time interval to reconstruct the hammer force successfully, under the condition that the seventh pulse reaches the sensor after extinction of the first pulse. However, it turns out that such a six-wave scheme is unstable. The idea used here is to consider eight waves (instead of six), because it yields again a stable filter. This procedure does not affect the result of the reconstruction: the output signal obtained is then made of the reconstructed pulse of width τ_H followed by a varying number of zeroes, depending on the note. Another argument for this eight-wave scheme is that it remains valid under the condition

$$2L < c\tau_H < 4L, \quad (5)$$

which, in practice, is fulfilled for the remaining upper part of the piano (notes C6 to C8). As for the four-wave scheme, the

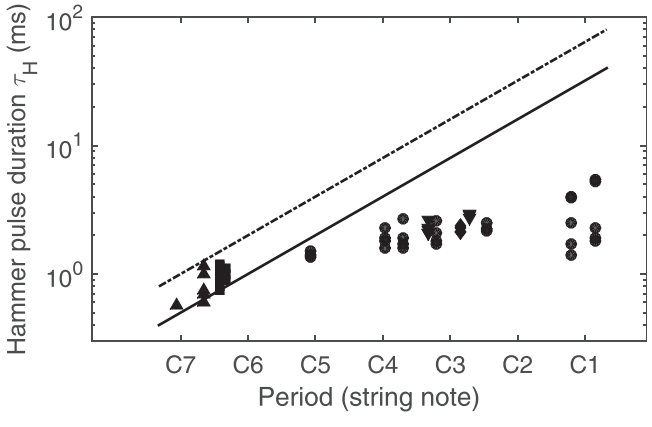

FIG. 3. Comparison between measured hammer pulse duration τ_H and period $T_1 = 1/f_1$ of the notes for different striking forces on various modern and historic keyboards: J. B. Streicher 1873 (●), Bösendorfer 1960 (■), Steinway D 1977 (▲), C. Graf 1828 (▼), N. Streicher 1819 (◆). Solid line: $\tau_H = T_1$, dashed-dotted line: $\tau_H = 2 \times T_1$. The x-axis is in log-scale, each octave corresponding to a period doubling. The period for the note C6 is roughly equal to 1.0 ms.

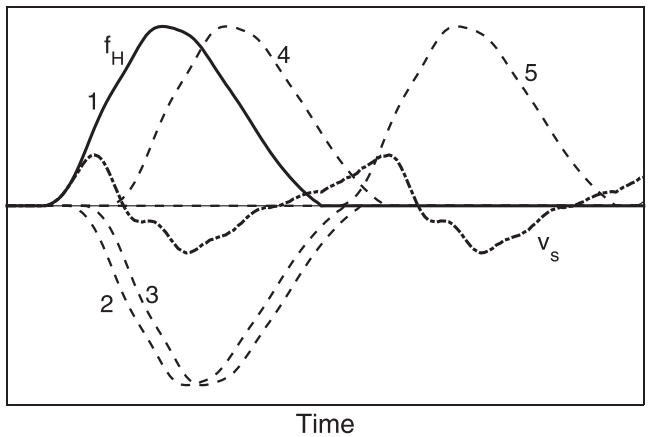

FIG. 4. Fourwaves scheme. Configuration $x_s > x_H$. In this example, four pulses are involved during the initial time τ_H corresponding to the width of the force pulse 1. This initial pulse goes to zero before the fifth reflected wave reaches the sensor. As a consequence, one can completely reconstruct the force from the string velocity by means of a four-wave scheme.

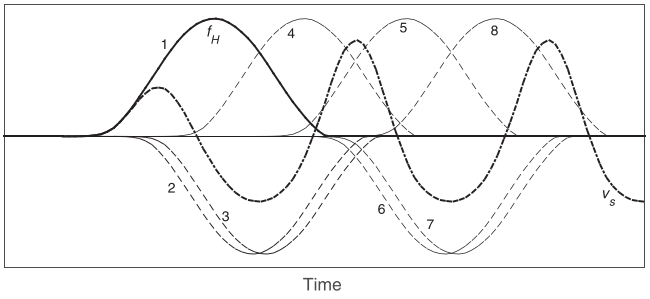

FIG. 5. Eight-wave scheme. Configuration $x_s > x_H$. In this example, the initial pulse goes to zero before the seventh wave reaches the sensor. However, due to stability reasons, a slightly larger time interval of v_s will be considered to reconstruct the force, where the velocity is represented by the eight first incoming and reflected waves.

properties of the corresponding filter imposes to select x_s close to the bridge (see Sec. II C). In summary, the force reconstruction is governed by two important criteria. In the time-domain, the width τ_H of the hammer force pulse imposes the number of waves to consider in the inverse filtering. In the frequency-domain, the properties of the reconstruction filter impose the location of the measuring point x_s along the string, as shown below in Sec. II C.

C. Reconstruction filters

1. General formulation

The string wave propagation qualitatively presented in Sec. II B can be formally described by a filter with the hammer force as input signal, and the string velocity at the measuring point as output signal. For discrete signals sampled at frequency $f_e = 1/T_e$, the appropriate tool is the z-transform where a delay of T_e corresponds to a multiplication by z^{-1}. Therefore z^{-m} corresponds to a delay of m samples, that is, mT_e seconds. For details on the z-transform, see, for example, Ref. 12. In what follows, $V_s(z)$ and $F_H(z)$ denote the z-transforms of $v_s(t)$ and $f_H(t)$, respectively. In the Appendix, the example of a plucked string with a pickup output developed by Karjalainen *et al.* is adapted to the present piano case.[13] For a lossless nondispersive string, it is shown that the transfer function between string velocity and hammer force is given by

$$H_{VF}(z) = \frac{V_s(z)}{F_H(z)} = \frac{z^{-n_1}}{2Z_c}\frac{(1-z^{-m_1})(1-z^{-m_2})}{(1-z^{-m_3})}, \tag{6}$$

where n_1 accounts for the propagation delay between hammer and sensor, m_1 and m_2 account for the delays due to hammer and sensor positions, and m_3 is the delay for one complete loop. Conversely, if $V_s(z)$ is known, the hammer force $F_H(z)$ can be retrieved through the inverse transfer function

$$H_{FV}(z) = \frac{F_H(z)}{V_s(z)} = 2Z_c\frac{z^{n_1}(1-z^{-m_3})}{(1-z^{-m_1})(1-z^{-m_2})}. \tag{7}$$

If the sensor is situated on the left-hand side of the hammer (on the agraffe side: $x_s < x_H$), it is shown in the Appendix that

$$n_1 = \frac{(x_H - x_s)f_e}{c}; \quad m_1 = \frac{2x_s f_e}{c} = \frac{x_s f_e}{Lf_1};$$
$$m_2 = \frac{(L - x_H)f_e}{Lf_1}; \quad m_3 = \frac{f_e}{f_1}. \tag{8}$$

Conversely, for $x_s > x_H$ (sensor on the bridge side), the delay constants are obtained through permutation of x_s and x_H

$$n_1 = \frac{(x_s - x_H)f_e}{c}; \quad m_1 = \frac{2x_H f_e}{c} = \frac{x_H f_e}{Lf_1};$$
$$m_2 = \frac{(L - x_s)f_e}{Lf_1}; \quad m_3 = \frac{f_e}{f_1}. \tag{9}$$

2. Approximate two-, four-, and eight-wave filters

The transfer function expressed in Eq. (7) is valid for an infinite number of waves reaching the sensor. The filters corresponding to the wave analysis presented in Sec. II B are obtained by truncating this expression to the initial portion of the signal. Considering the first two incoming waves only, then H_{FV} reduces to

$$\begin{cases} H_{FV2w}(z) = 2Z_c\dfrac{z^{n_1}}{1-z^{-m_1}} & \text{for } x_s < x_H, \\ \text{or} & \\ 2Z_c\dfrac{z^{n_1}}{1-z^{-m_2}} & \text{for } x_s > x_H. \end{cases} \tag{10}$$

Notice that the first expression in Eq. (10) is the transfer function directly obtained by taking the z-transform of Eq. (2). Similarly, a four-wave approximation is given by

$$H_{FV4w}(z) = 2Z_c\frac{z^{n_1}}{(1-z^{-m_1})(1-z^{-m_2})}. \tag{11}$$

Finally, for the eight-wave scheme, the corresponding filter is obtained by approximating the factor $(1-z^{-m_3})$ by the two first terms of its expansion, which yields

$$H_{FV8w}(z) = 2Z_c\frac{z^{n_1}}{(1-z^{-m_1})(1-z^{-m_2})(1+z^{-m_3})}. \tag{12}$$

Notice, in this case, that Eq. (7) can be used alternatively instead of Eq. (12). The advantage is then to deal with the feed-forward filter $1-z^{-m_3}$ rather than with the feedback version $1/(1+z^{-m_3})$, which adds high peaks in the spectrum.

After filtering of the velocity, the hammer force pulses are obtained by truncating the signal in time below the upper limit of validity for each of the three schemes given in Eqs. (3)–(5). Using the general form of the inverse filter Eq. (7) theoretically yields an infinite domain of validity in time. However, in practice, due to the presence of noise and progressive departure from the underlying model when dealing with real signals, the filtered velocity again has to be truncated to reasonable values. An upper bound of 10 ms is, in general, sufficient for recovering the force.

3. Selection of the measurement point x_s

Some precautions should be taken in using the previous filters to reconstruct the hammer force. This is due to the fact

that both delays m_1 and m_2 now introduce comb filtering effects with poles at frequencies $f_{km_1} = kf_e/m_1$ and $f_{km_2} = kf_e/m_2$, respectively. Because of their high gain, these pole frequencies can perturb the reconstruction of the force if they are smaller than the upper limit f_{VM} of the velocity spectrum. These perturbations are due to amplification of noise and deviations from the ideal case in real signals at these frequencies. Therefore, given the expressions of m_1 and m_2 in Eqs. (8) and (9), the appropriate strategy for limiting these perturbations is to select x_s so that f_{VM} is smaller than the lowest poles fe/m_1 and f_e/m_2, which yields the following conditions:

$$\begin{cases} \text{for } x_s < x_H: & \dfrac{x_s}{L} < \dfrac{f_1}{f_{VM}} \quad \text{and} \quad \dfrac{L - x_H}{L} < \dfrac{f_1}{f_{VM}}, \\ \text{for } x_s > x_H: & \dfrac{x_H}{L} < \dfrac{f_1}{f_{VM}} \quad \text{and} \quad \dfrac{L - x_s}{L} < \dfrac{f_1}{f_{VM}}. \end{cases} \tag{13}$$

For $x_s < x_H$, the second condition, relative to m_2 in Eq. (13) is unacceptable since it implies that the spectrum of the string velocity should be limited to the fundamental frequency. Therefore, only the condition on m_1 remains, which means that this configuration is valid for the two-wave scheme only. According to the wave analysis presented in Sec. II B, this scheme is applicable to the bass and medium range of the piano. In this range, x_s must be small compared to L (sensor close to the agraffe) so that the poles of the filter are rejected out of the velocity spectrum. With $x_s/L = 100$, for example, the lowest pole of the filter is rejected beyond the 100th harmonic of the string.

The configuration $x_s > x_H$ is applicable to four- and eight-wave schemes if the two corresponding conditions in Eq. (13) are fulfilled. From the wave analysis in Sec. II B, we know that such schemes are applicable in the treble range between C5 and C8. The second condition on m_2 implies that x_s is close to L, which is obtained now by placing the sensor close to the bridge. In practice, good results are obtained for $0.05 < (L - x_s)/L < 0.1$. The first condition related to x_H/L is imposed by the construction of the piano. On average $x_H/L = 0.1$, which means that the lowest pole frequency of the reconstruction filter is rejected beyond the tenth harmonic. Usual piano tones show relatively little energy beyond this harmonic, between C5 and C8 (see, for example, Fig. 11), and thus the configuration $x_s > x_H$ is valid in this range. Notice also that the regularization presented in Sec. II C 4 allows to reduce the perturbating effects of the poles.

4. Further considerations: Dispersion, fractional delays and regularization

In the bass range of the piano, it becomes necessary to account for the dispersion of the wave due to string stiffness. One widely used method for this is to divide the transfer function $H_{VF}(z)$ in Eq. (6) by an appropriate allpass filter $D(z)$ whose phase and delay properties are based on the physical parameters of the string. For a stiff string, the phase shift $\varphi(f)$ for a roundtrip is given by[14]

$$\varphi(f) = -\frac{2\pi f}{f_1} \frac{1}{\sqrt{1 + B\dfrac{f^2}{f_1^2}}}, \tag{14}$$

where $B = \pi^2 EI/T_0 L^2$ is the stiffness coefficient. The associated group delay $\gamma(f)$ is given by

$$\gamma(f) = \frac{1}{f_1} \frac{1}{\left[1 + B\dfrac{f^2}{f_1^2}\right]^{3/2}}. \tag{15}$$

The pertinent dimensionless coefficient here is $\varepsilon_s = Bf^2/f_1^2$ which, for a given frequency f, continuously decreases from bass to treble. For reproducing this delay, a set of eight biquad filters in cascade was applied, following the method proposed by Abel *et al.*[14,15]

The delays defined in Eqs. (8) and (9) are usually not integers. Therefore one useful strategy is to use fractional delay filters to represent them. Here, Thiran allpass filters were tested successfully.[16] Oversampling is another strategy, so that approximating n_1, m_1, m_2, and m_3 by the nearest integers yields a small error. Both methods gave comparable results.

Finally, a regularization can be made in replacing $(1 - z^{-m_1})$ and $(1 - z^{-m_2})$ by $(1 - g_1 z^{-m_1})$ and $(1 - g_2 z^{-m_2})$ in Eq. (7), with $0.99 < g_1, g_2 < 0.999$, so that the gain of $H_{FV}(z)$ does not tend to infinity at those frequencies. The consequences on the pole frequencies are negligible. Physically, such a regularization accounts for a slight dissipation at both ends of the string. The interval of values of g_1 and g_2 are selected somewhat arbitrarily, but the examples shown in Secs. III and IV show that this has no appreciable effect on the amplitude of the reconstructed force. However, selecting g_1 and g_2 smaller than 0.99 (which would correspond to losses at the ends higher than 1%) generally leads to unwanted drift in the reconstructed force waveform, showing that the corresponding damping at the string ends is then probably overestimated. Notice that, for coherence, the factor $(1 - z^{-m_3})$ must be then replaced by $(1 - g_1 g_2 z^{-m_3})$. In conclusion, after inversion, the most general formulation of the transfer function used for reconstructing the hammer force is written

$$H_{FV}(z) = \frac{F_H(z)}{V_s(z)} = 2Z_c \frac{z^{n_1}(1 - g_1 g_2 z^{-m_3})D(z)}{(1 - g_1 z^{-m_1})(1 - g_2 z^{-m_2})}, \tag{16}$$

where the delays are implemented with fractional delay filters.

III. APPLICATION TO SIMULATED PIANO STRINGS

In this section, the method of hammer force reconstruction presented in Sec. II is tested on simulated piano strings. Using string simulations allows a perfect control on the input hammer force and careful comparison with the reconstructed force. In addition, the influence of the main causes of departure from the ideal string case on the quality of the reconstruction can be tested and quantified separately, which is not possible on real strings. Specifically, we take benefit of the simulation model to test the influence of absorption,

dispersion, and non-linearity of the string wave propagation on the resulting hammer force reconstruction. The waves schemes presented in Sec. II (two-, four- and eight-waves, respectively) are tested in the different note ranges of the keyboard of various pianos: bass, medium, and treble, and for different striking forces (p,mf,f). The reconstructed hammer force is obtained by filtering the simulated string velocity at a given sensor position x_s.

A. Model and method

The string model used for the simulations is a part of a complete numerical piano model developed by Chabassier *et al.*[8,17] This model will not be detailed further here, since it has been presented in these previous papers extensively. For the string part, this model includes damping, stiffness, and nonlinear terms. The frequency-dependent damping is classically modeled by two-terms: a so-called "fluid" term and a "viscoelastic" damping term for each component of the string motion. The stiffness term is obtained by modeling the string as a prestressed beam. The additional nonlinear terms account for the influence of the amplitude on the string motion.[18] The transverse motion of the string is assumed here to be vertical (in the direction of the hammer force) and coupled to its longitudinal motion. The motion of both ends (agraffe and bridge) is ignored in the description used here. The values of the parameters are derived from measurements on real strings (see Table I).

In the simulations presented in this section, the hammer forces are given as input data. The amplitude, duration, and shape of the imposed force pulses are selected as close as possible to the reality. In some cases, the hammer mass and acceleration were measured on real strings beforehand and, thus, the input force is obtained by multiplying together these two quantities. In the other situations, the string-hammer coupling is modeled by a standard power law in which the coefficients are adjusted in order to obtain realistic hammer force amplitude and duration.[19,20] As it has been already pointed out by several authors,[3,6] and as discussed further in Sec. IV of this paper, we are aware of the fact that these input hammer pulses might differ from the real forces, either because of several causes of experimental errors (hammer misalignment, vibrations of the hammer shank,…), or because of the approximate modeling by a power law.[5] However, these differences do not invalidate the testing of the reconstruction procedure presented here. In fact, this reconstruction is supposed to account for any hammer pulse, provided that the linear theory presented in Sec. II is applicable, and for the appropriate wave filter (two-waves, four-waves, or eight-waves) compatible with the pulse duration τ_H.

In Sec. III B, it is analyzed to what extent realistic departures from the "ideal linear string," in terms of absorption, dispersion, and nonlinear propagation, can affect the reconstruction of the hammer force. A systematic study of the influence of each of these perturbation terms is presented. In Sec. III C, representative examples of hammer force reconstruction are presented in the three main ranges of the piano: bass, medium, and treble, using the appropriate waves schemes.

TABLE I. String parameters used in the simulations. JBS73, JBS50, and JBS36: J. B. Streicher pianos made in 1873, 1850, and 1836, respectively; BSD: Bösendorfer piano (1960); Φ: core diameter, NM: not measured.

Note	D♯1	D♯1	F♯2	C4	C♯5	C♯5	D♯6	E6
Piano	JBS73	JBS50	JBS73	JBS73	JBS36	JBS73	BSD	BSD
L (m)	1.717	1.710	1.57	0.65	0.261	0.335	0.165	0.137
Φ (mm)	1.25	1.1	1.14	0.94	0.73	0.885	0.80	0.80
T_0 (N)	781.6	520	598	552.6	267.9	593	680.5	522.8
f_1 (Hz)	36	37	87	245	547	523	1258	1328
m_H (g)	5.9	NM	5.4	4.8	NM	4.2	7.02	6.96
x_H (mm)	190	180	165	75	28	42	20	17
x_s (mm)	10	9	27	15	14	325	156	127
$\mu = \rho A$ (g m^{-1})	51.1	32.5	8.01	5.45	3.22	4.83	3.95	3.95

$A = \frac{\pi\Phi^2}{4}$, $I = \frac{\pi\Phi^4}{64}$, $E = 2.0 \times 10^{11}$ Pa

B. Effects of some causes of departure from the ideal string on the reconstructed force

1. Absorption and damping

Consider a string with fundamental frequency $f_1 = 1/T_1$ and frequency-dependent time-constant $\tau(f)$ due to damping. For each partial n, the attenuation due to damping during a roundtrip is proportional to $1 - \exp[-T_1/\tau(f_n)]$, which, for $T_1 \ll \tau$, reduces to T_1/τ. An order of magnitude can be obtained by calculating this attenuation around the mid-frequency $f_m = 1$ kHz. As an example, we measured $\tau(f_m) = 1.2$, 0.7, and 0.2 s, for the three strings D♯1, C4, and E6 examined here. This yields an attenuation of 2.3%, 0.6%, and 0.4%, respectively, for one roundtrip on these three strings. In practice, the observed attenuation is smaller than these limits (<1%) since the distance traveled by the wave is less than twice the string length (see Fig. 6). As a consequence, no correction was applied here since the attenuation error is weak compared to the other sources of error. Notice however that, if necessary, an additional filter can easily be designed for compensating the frequency-dependent damping along the string.[21]

2. Dispersion due to stiffness

At $f = 1$ kHz, the stiffness coefficient ε_s defined in Sec. II C takes the values 7.9×10^{-2} for the string D♯1, 1.28×10^{-2} for the string C4, and 2.3×10^{-3} for the string E6. This results in group delays (normalized to the period) equal to 0.12, 1.9×10^{-2}, and 3.4×10^{-3}, respectively, for strings D♯1, C4, and E6. As a consequence, dispersive effects are clearly seen on velocity waveforms for the strings in the bass range, which results in a distortion of the wave, even for reduced propagation distances on the order of x_H (see Fig. 6). For the two lowest octaves of most pianos, it was thus necessary to design allpass filters in order to compensate for this dispersion (see Fig. 12). The dispersive effects decrease rapidly with the key number, and do not alter the reconstruction of the force for the notes above A2 in all observed pianos.

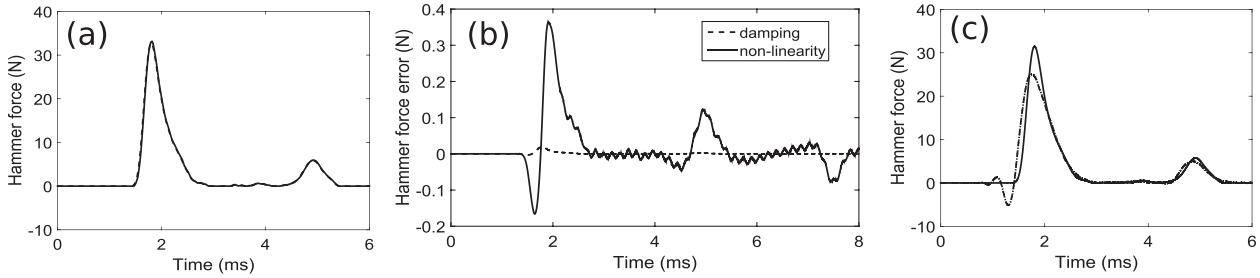

FIG. 6. Hammer force reconstruction in the bass range. Two-wave scheme. J. B. Streicher piano (1873): note D♯1 (fundamental 36 Hz). (a) Comparison between input force (solid) and force reconstructed from a simulated ideal string. (b) Differences in the reconstructed force due to damping (dashed) and non-linearities (solid). (c) Comparison between input force (solid) and force reconstructed from a simulated stiff string (dashed-dotted line).

3. Amplitude non-linearity

An appropriate strategy for evaluating the influence the non-linearity due to the amplitude of the string motion is to examine the nonlinear vibrating equation, which, to a first-order expansion, can be written as[22]

$$\frac{\partial^2 y}{\partial t^2} \approx c^2 \frac{\partial^2 y}{\partial x^2}\left[1 + \frac{3}{2}\frac{c_L^2}{c^2}\left(\frac{\partial y}{\partial x}\right)^2\right], \tag{17}$$

where $c_L^2 = EA/\mu$ is the longitudinal wave speed in the string of cross-sectional area A and linear density μ. An order of magnitude for the derivative $\partial y/\partial x$ is given by the ratio V/c between the amplitude of the string velocity V and the transverse speed c. In total, the relevant dimensionless non-linearity coefficient can be written

$$\varepsilon_{\mathrm{NL}} = \frac{3}{2}\frac{EA}{T_0}\frac{V^2}{c^2}. \tag{18}$$

This coefficient quantifies the change in transverse speed due to the amplitude of the wave, which might induce some distortion. Here, again, $\varepsilon_{\mathrm{NL}}$ regularly decreases as the pitch of the note (or, equivalently, the key number) increases. For $V = 1$ m/s (which, in most cases, corresponds to a *mezzoforte* level), $\varepsilon_{\mathrm{NL}}$ takes the values 2.39×10^{-2}, 3.7×10^{-3}, and 2.83×10^{-3} for the three strings D♯1, C4, and E6, respectively. In practice, the effects of non-linearity on the force reconstruction were observed in the low bass range only, for V higher than 1 m/s (see Fig. 6). Notice that Eq. (17) accounts for the transverse effects of the amplitude non-linearity only, which is equivalent to a modulation of tension. The general nonlinear model used here for the simulations also accounts for the longitudinal component of the string, which is not measured by the sensor.

In summary, the above dimensionless analysis of the three "perturbation" terms (damping, stiffness, amplitude non-linearity) in the ideal string wave equation shows that stiffness is likely to be the main cause of errors in the force reconstruction. Nonlinear and damping effects are much weaker, although the errors due to non-linearity might rapidly increase with amplitude, since they are proportional to the square of the string velocity. Another important result of this analysis is that the effects of these perturbation terms regularly decrease with the fundamental frequency of the note. It is therefore expected that they are dominant in the bass range. The consequences on the reconstruction of the hammer force are shown in Sec. III C for some simulated notes in the bass, medium, and treble ranges of the piano.

C. Examples of reconstructed hammer forces

1. Bass range. Two-wave scheme

Figure 6 shows an example of reconstructed hammer force for the string D♯1 of a pianoforte made by J. B. Streicher in 1873 (JBS73). The excitation corresponds to a level between *forte* and *fortissimo*, with a maximum force of 32 N, and a maximum string velocity of $V = 2.5$ m/s. A two-wave scheme is applied. Figure 6(a) shows that the reconstructed force perfectly coincides with the input force for a simulated ideal string. The errors (in N) due to damping and nonlinear terms are shown in Fig. 6(b). The maximum discrepancy due to the damping terms is 0.02 N, with corresponds to a relative error of 6.0×10^{-4}, and can be ignored. The maximum error due to the presence of nonlinear terms in the string wave equation is equal to 0.36 N, or 1.13% in relative value. This error is comparable to other potential causes of errors encountered in the application of the method to real strings (see Sec. IV). Finally, Fig. 6(c) shows the effects of stiffness on the reconstructed force. In this case, the consequences of the dispersion are clearly seen, resulting in an underestimation of the maximum force (around 20% here), a slight broadening of the pulse, and the presence of characteristic oscillations in the onset. The results presented here are representative of those observed in the two lowest octaves of the investigated pianos. The discrepancies due to stiffness and non-linearity increase when approaching the lowest notes of the keyboard. They decrease when moving to the higher keys and, in general, as the amplitude of the hammer force decreases.

2. Medium range. Two-wave scheme

In this paragraph, representative examples of hammer force reconstruction in the medium range of the piano are presented. This range covers nearly three octaves (from note E2 to C5). In this interval of notes, a two-wave reconstruction scheme is applied. The string parameters and the input force pulses are derived from measurements performed on a JBS73 piano (see Table I). In Fig. 7, the input forces (solid lines) and the reconstructed forces (dashed lines) are shown for the notes F♯2 (fundamental 87 Hz) and C4 (fundamental

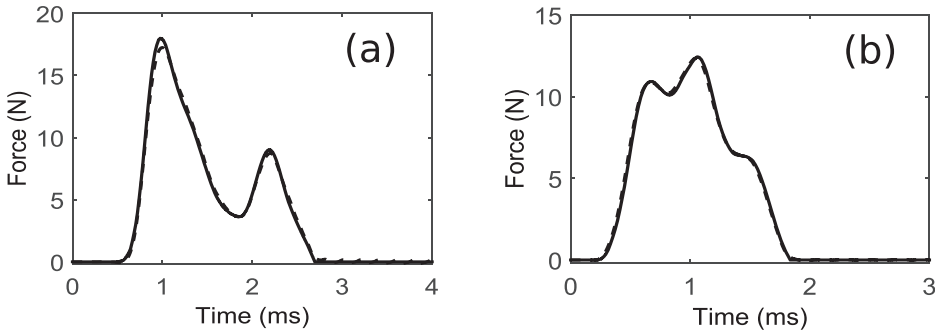

FIG. 7. Force reconstruction in the medium range. Two-wave scheme. Piano J. B. Streicher (1873). (a) Note F♯2, mezzoforte, $f_1 = 87$ Hz. (b) Note C4, forte, $f_1 = 245$ Hz. Solid line: input force. Dashed line: reconstructed force.

245 Hz). The reconstruction is made with the complete string model, including damping, stiffness, and nonlinear terms. It can be seen that the hammer forces are very well reproduced in each case. The amplitudes, time duration, and shapes of the reconstructed forces coincide with those of the input forces almost exactly. This means that the different causes of departure from the "ideal" string integrated in the simulation model do not affect the wave propagation substantially. As a consequence, the effects of the additional terms (damping, stiffness, non-linearity) remain small. However, one exception should be underlined: as seen in Fig. 7, the first pulse of the reconstructed hammer force for the note F♯2 shows a slightly more rounded profile than the input force, which results in a smaller amplitude by a few percent. This discrepancy is due to the dispersive effects of stiffness.

3. Treble range. Four- and eight-wave schemes

Finally, reconstructed forces are presented here for the notes in the upper part of the keyboard. This range corresponds to the domain of notes where the period becomes smaller than the width of the hammer pulse, as shown in Fig. 3. In this domain (with pitch higher than C5 for most pianos), four- and eight-wave schemes must be applied for reconstructing the hammer force. Figure 8 shows two examples of reconstruction with the complete string model. The hammer force of the C♯5 string is reconstructed with a four-wave scheme, while the E6 force is reconstructed with an eight-wave scheme. In both cases, no differences can be seen between input and reconstructed forces, which means that the perturbation terms have no visible effects.

In conclusion of this section, it is confirmed that the hammer forces can be reconstructed from simulated string velocities generated by a model that includes damping, stiffness, and nonlinear terms in addition to the main inertial and tension terms. Depending on the notes, two-, four-, or eight-wave filters must be applied to the string velocity to recover the hammer force. As shown in Sec. II, the choice of the filter depends on the ratio between the period of the string oscillation and the duration of the hammer pulse. In the low bass range, corresponding to the two lowest octaves for most pianos, dispersion effects due to stiffness are more pronounced, which alters the quality of the reconstruction. In this case, the dispersion needs to be corrected by the use of an allpass filter whose parameters are derived from the physical parameters of the string, as seen in Sec. II C.

Due to the relatively small distance traveled by the waves along the string during its transient oscillation, the other causes of departure from the "ideal" "string" (damping, non-linearity) induce only small effects in the reconstruction of the hammer force: the duration and shape of the pulse are not affected, and its magnitude is estimated within a few percent, or less, compared to the input force.

IV. APPLICATION TO MEASURED PIANO STRINGS

After validation on simulated string waveforms, this section shows some results obtained with the hammer force reconstruction method applied to real piano strings. In addition to damping, stiffness and non-linearities, other physical phenomena, might alter the quality of the force reconstruction. The coupling between the strings of a given note, the whirling motion of the string, and lack of accuracy in the velocity measurements, for example, might lead to wrong estimations. Therefore, it is challenging to test whether the proposed method is robust enough against these potential causes of errors.

The general procedure is shown in Fig. 9. In the most general case (case 1), the hammer force is not known. The hammer force $f_{\mathrm{HR}}(t)$ is then reconstructed through filtering of the measured string velocity $v_{\mathrm{sm}}(t)$, following the method

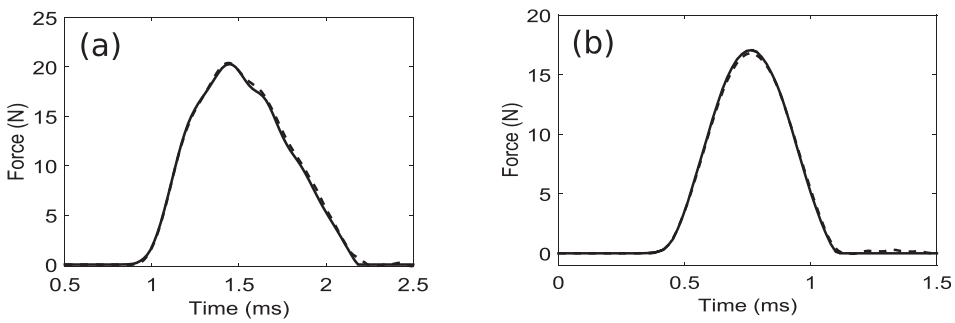

FIG. 8. Force reconstruction in the treble range. (a) Piano J. B. Streicher 1873: string C♯5, four-wave scheme. (b) Bösendorfer: string E6 eight-wave scheme. Comparison between input force (solid) and reconstructed force (dashed).

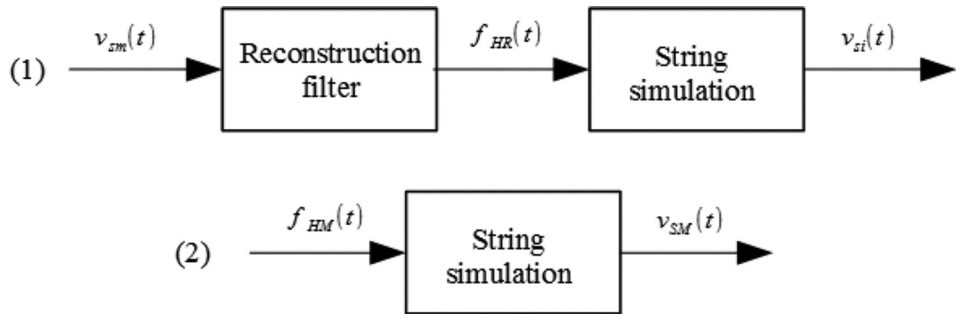

FIG. 9. Validation procedures of the hammer force reconstruction method. Case (1) Through appropriate filtering, the measured string velocity $v_{sm}(t)$ yields the reconstructed hammer force $f_{HR}(t)$. This force is used as input force in the string simulation model, which yields the simulated string velocity $v_{si}(t)$, for comparison with $v_{sm}(t)$. Case (2) If the hammer force $f_{HM}(t) = m_H a_H(t)$ is measured, another string simulation $v_{SM}(t)$ is performed with this force as input excitation, and compared with both $v_{sm}(t)$ and $v_{si}(t)$. Further comparison is made between reconstructed $f_{HR}(t)$ and measured $f_{HM}(t)$ forces.

presented in Sec. II. This force is used as input data in the string simulation model presented in Sec. III, which yields the simulated string velocity $v_{\mathrm{si}}(t)$, for further comparisons with $v_{\mathrm{sm}}(t)$, as shown in Sec. IV B. In the present study, an estimation of the measured hammer force $f_{\mathrm{HM}}(t)$ was also derived in some particular cases from measurements of mass and acceleration of the hammer head. In these cases (case 2), this measured hammer force is compared to the reconstructed force, and also serves as input data in the string simulation model, in order to compare the resulting string velocity $v_{\mathrm{SM}}(t)$ to both $v_{\mathrm{sm}}(t)$ and $v_{\mathrm{si}}(t)$. This second procedure is detailed in Sec. IV C. The section ends with an example of application of the method to the case of an historic piano with a Viennese action.

A. Measurements

Figure 10 shows a picture of the setup used for measuring the string velocity. The sensor is a standard electromagnetic transducer made of a coil wound onto a small cylindrical permanent magnet, similar to an electric guitar pickup, and placed in the vicinity of the string. This transducer delivers a voltage proportional to the vertical component of the string velocity. The distance between the magnet and the string is adjusted with a micrometer screw. The sensor and the screw can slide from string to string along a horizontal metallic bar placed over the instrument. A calibration procedure is made prior to the measurements, where the signal delivered by the transducer is compared to the output of a laser vibrometer Polytec IVS-400 (Hörsching, Austria). The efficiency of the transducer (in mV/m/s) is tested against string amplitude, frequency, and sensor-string distance. The efficiency is constant for a string amplitude between 20 and 300 μm, and shows a slight increase of 5% between 0.3 and 1.0 mm. In our experiments, the sensor is placed either close to the bridge or to the agraffe, so that the string amplitude is $<200\,\mu$m.

B. Comparison between measured and simulated string velocity

We show here some representative results of the force reconstruction method applied to measured string velocities. This is supposed to correspond to the standard, and most useful, application of the method. In the absence of measured hammer force, the validity of the reconstructed force is tested by comparing the measured string velocity with simulations where the input signal is the reconstructed force (see Fig. 9).

Figure 11 shows the results of the hammer force reconstruction method applied to the string C♯5 of a J. B. Streicher piano built in 1836 (JBS36). It can be seen that the string velocity simulated with the reconstructed force reproduces the measured waveform almost perfectly, even on a large time scale. This is confirmed by the spectral analysis performed on the first 50 ms of the signal, which shows a high degree of coincidence between 0 and 5 kHz. A DC-component at -30 dB below the maximum can be seen on the measured spectrum.

In the bass range, an allpass filter is applied to the measured string velocity in order to compensate for the dispersion due to stiffness. Figure 12(b) shows the effect of this

FIG. 10. Experimental setup. The string velocity is measured with an electromagnetic transducer placed near the string. The string-sensor distance is adjusted with a micrometer screw. The sensor and the screw-holder can slide from string to string along a metallic bar.

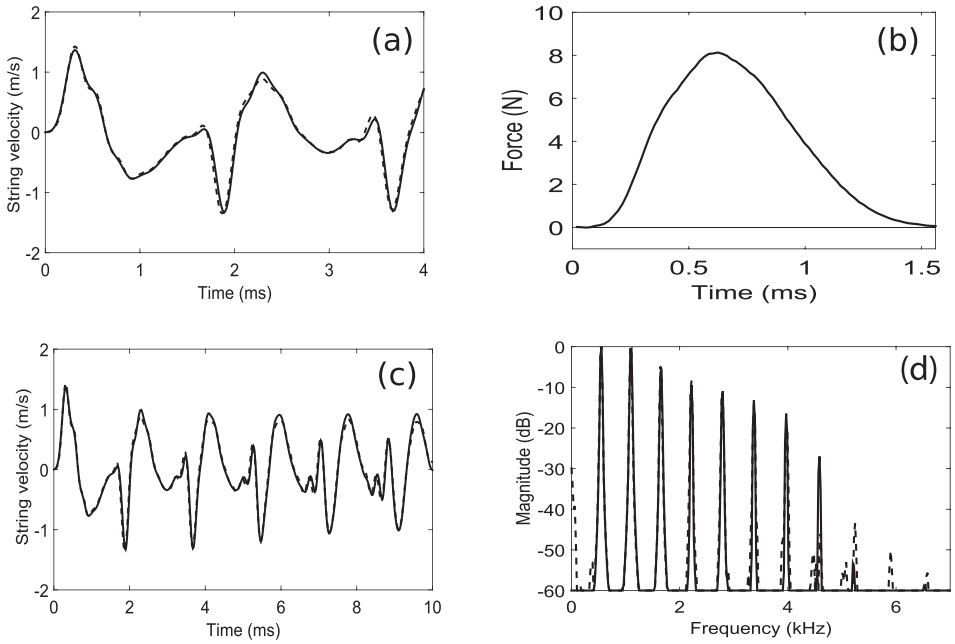

FIG. 11. Hammer force reconstruction method applied to the measured string C♯5 of a J. B. Streicher piano (1836) with a two-wave filter. (a) Comparison between measured (dashed line) and simulated (solid) string velocity. (b) Reconstructed force pulse used as input for the simulations. (c) Extended comparison between measured (dashed) and simulated (solid) string velocity (10 ms), and corresponding spectra.

filter on the hammer pulse when the dispersion is reduced, which is comparable to the results obtained on the simulations in Sec. III C when the stiffness term is removed from the string equation. The string velocity simulated with the filtered reconstructed force shows a good agreement with the measured velocity over a large time scale (35 ms) despite some discrepancies in the amplitudes of some sub-oscillations. These discrepancies could be due to some inaccuracy in the modeling of the frequency-dependent damping, always a delicate task, especially in the bass range. However, the comparison between the two corresponding spectra shows an excellent agreement. The major differences are seen at the peaks of small amplitudes, around -20 dB below the maximum (0 dB), and can be attributed either to some small errors in the estimation of the string parameters (damping) or in the measurements (precise location of the string sensor).

C. Comparison between reconstructed and measured force

Figure 13 shows an example of hammer force reconstructed from measurements of the string velocity for the note F♯2 of a J. B. Streicher piano (1873). The reconstructed force is compared to the measured force derived from measurements of mass and acceleration of the hammer head. One can see that measured and reconstructed forces coincide during the first pulse of the waveform. However, some differences exist in the magnitude of the second pulse. In addition, the measured force tends faster to zero and the remaining oscillations of the hammer head are clearly visible. Both forces are used as input forces for simulating the string velocities, using the measured parameters shown in Table I. The simulated string velocities are then compared to the measured velocity. Here, again, one can see an excellent agreement between the measured velocity and the velocity

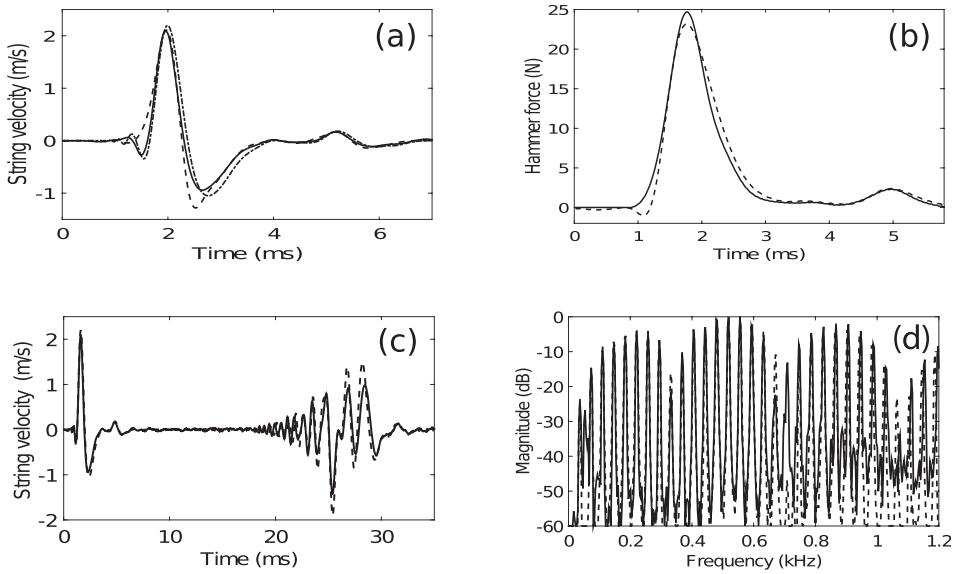

FIG. 12. Hammer force reconstruction applied to the string D♯1 of a J. B. Streicher piano made in 1850 (JBS50). Two-wave scheme. (a) Comparison between measured string velocity (solid), velocity reconstructed with (dashed), and without (dashed-dotted) allpass filtering. (b) Comparison between hammer force reconstructed without (dashed) and with (solid) allpass filtering. (c),(d) Large-scale comparison between measured (solid) and simulated velocity with filtered force and corresponding spectra.

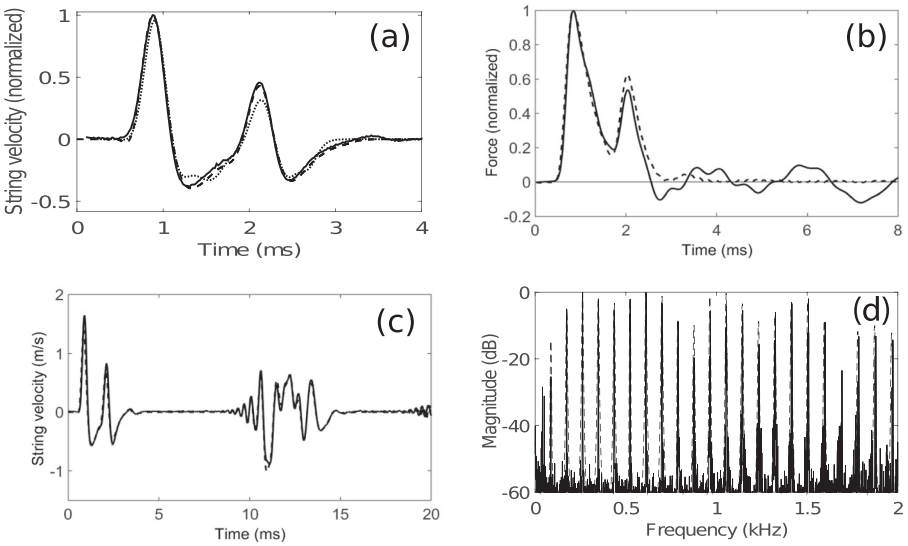

FIG. 13. Hammer force reconstruction method applied to the string F♯2 of a J. B. Streicher piano (1873) with a two-wave filter. (a) Comparison between measured velocity (solid line), simulated velocity with reconstructed force (dashed), and velocity simulated with the measured force (dotted); (b) reconstructed force pulse used as input for the simulations (dashed), and comparison with the hammer force derived from measured mass and acceleration of the hammer (solid). (c) Extended comparison between measured (solid) and simulated (dashed) string velocity (20 ms) and corresponding spectra.

simulated with the reconstructed force, even on a long period of time. The simulations performed with the reconstructed force as input quantity yields waveforms and spectra closer to the measurements than the simulations using measured hammer head acceleration and mass at the input. This is not surprising since the reconstruction filter does not take the vibrations of the hammer shank into account.

In the treble range, Fig. 14 shows the results of the hammer force reconstruction method applied to the string D♯6 of a Bösendorfer piano with an eight-wave filtering scheme. The comparison between the reconstructed force and the measured force obtained through multiplication of mass and acceleration of the hammer head again shows that this latter is affected by the oscillations of the head + shank system, resulting in differences in duration and shape of the main pulse. Again, and for the same reasons as previously, the string velocity simulated with the reconstructed force shows a better agreement with the measured velocity that the velocity simulated with the measured force truncated to its first positive pulse. This agreement is confirmed by observing the velocities over a larger period of time (8 ms) and on the spectra, where only small differences are visible below 5 kHz.

In summary, comparing the hammer pulses derived from the present method with hammer head mass-acceleration measurements shows that the present method is insensitive to the perturbing oscillations of the hammer shank. Its main advantage also follows from the fact that it does not need to have direct access to the hammer: this feature is of the utmost importance when measuring valuable and fragile instruments such as historic pianofortes.

D. Application to historic pianofortes

One running application of the present method is to investigate the evolution of hammer-string interaction in the history of piano making. In this respect, Fig. 15–(a) shows an example of a reconstructed hammer force (note D3) for a copy recently made by G. Hecher of a pianoforte built by Nanette Streicher in 1805 (GH05). This instrument uses a Viennese action,[23] and 200-yr-old leather is glued on the hammer heads. From the qualitative comparison with the

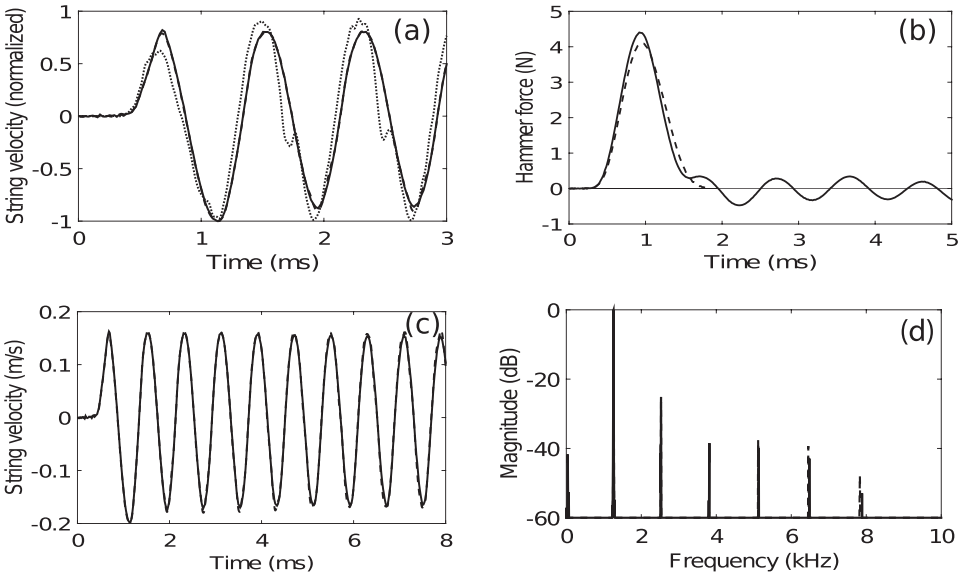

FIG. 14. Force reconstruction applied to a Bösendorfer piano with an eight-wave filter. Note D♯6. (a) Comparison between measured string velocity (solid), simulated velocity excited by the reconstructed force (dashed), and simulated velocity with the measured hammer force (mass × acceleration) at the input (dotted). (b) Comparison between measured (solid) and reconstructed (dashed) hammer force. (c) Comparison between measured (solid) and simulated string velocity (dashed) over 8 ms. (d) Spectra of measured (solid) and simulated velocity (dashed).

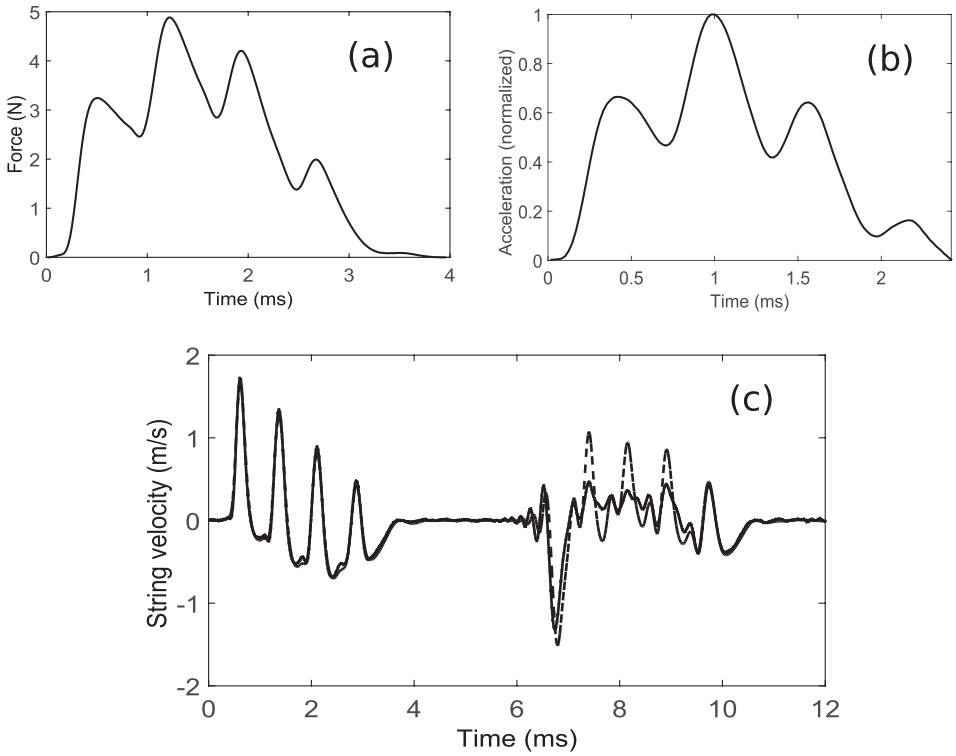

FIG. 15. (a) Force reconstructed for the note D3 of a piano built after an original pianoforte by N. Streicher (1805). (b) Hammer acceleration of a G3 note for a Steinway D (1977). (c) Comparison between measured (solid line) and simulated (dashed) string velocity for the N. Streicher-D3 note, showing the effect of the Viennese action in its second part.

hammer acceleration measured of a modern piano in the same half-octave (Steinway D, note G3) in Fig. 15(b), one can see that both shapes are globally similar. However, close observation shows some differences in the slopes and rounded profiles of the pulses, which are likely to be attributable to the respective behavior of leather and felt. Also interesting is the comparison between measured and simulated velocity for the GH05-D3 string in Fig. 15(c). The first part of both waveforms are identical, but significant differences now exist in the second part where the measured oscillations are significantly damped compared to the velocity simulated with the reconstructed force at the input. A very plausible explanation for this difference lies in the specificity of the Viennese action, where the hammer slips along the string before leaving it, a feature that is not taken into account in the reconstruction model.

V. CONCLUSION

In this paper, an original method was presented for reconstructing the piano hammer force from measurements of the string velocity. This method is based on the use of dedicated filters applied to the measured velocity. The design of these filters is derived from the analysis of wave propagation along a lossless linear string. For the five lowest octaves of a piano, a filter based on two-wave propagation (one incident and one reflected wave) is sufficient for reconstructing the hammer force. For the highest notes, a four- or an eight-wave scheme is necessary. The number of waves to consider is imposed by the duration of the hammer pulse. The velocity sensor must be placed either near the agraffe (two-wave scheme) or near the bridge (four- and eight-wave schemes) in order to ensure that the reconstructed force is not perturbed by the poles of the filter.

In a first step, the force reconstruction method has been validated on simulated piano strings, where the model includes absorbing, dispersive, and nonlinear terms. The input parameters of these simulations were derived from measurements on a large variety of historic and modern pianos. The results show that both the damping and nonlinear terms only have small effects on the estimation of the hammer force. On the contrary, the dispersion due to stiffness leads to significant discrepancies in the two lowest octaves, which needs to be compensated by means of a suitable allpass filter.

In a second step, the force reconstruction method is tested on velocity measurements performed on real piano strings. The measured string velocity is compared to the corresponding simulated velocity excited by the reconstructed force. It is found that the reconstructed hammer force yields a simulated string velocity that reproduces the measured velocity with a high degree of accuracy, both in time and frequency. This proves that the simplified string model used for designing the reconstruction filters accounts well for the observed wave propagation during the first oscillations after the hammer stroke. During this small time interval, known complicating effects, such as the whirling motion of the strings and the coupling between adjacent strings of the same note, are not yet initiated and do not perturb the reconstruction of the force. In this context, it would be of interest to compare the results with methods requiring the use of longer portions of velocity signal as, for example, those based on the use of direct and inverse Fourier transforms in the frequency domain. Comparisons of the reconstructed force with the results obtained by other experimental methods (such as optical methods and high-speed cameras) also remain to be done in order to completely assess the pertinence of the present filtering.

In some cases, the reconstructed force was compared to an estimate of the hammer force obtained by multiplying together the measured mass and acceleration of the hammer head. These comparison shows reasonable similarities in

terms of amplitude, shape, and duration, but differences are observed, which are mainly attributable to the oscillations of the hammer shank. Simulations of the string velocity performed with this measured force at the input of the present filters show more discrepancies than with the reconstructed force when compared to the measured velocity: such a result is not surprising if we consider that the dynamics of the shank are not included in the underlying model on which the reconstruction is based. In this context, extending the method to a filter with a transfer function between hammer acceleration and string velocity, which would include a model of shank, could be an interesting perspective.

Finally, the reconstruction method is applied to a copy of an historic piano equipped with a particular action (the so-called Viennese action). Qualitative comparison between the reconstructed force and the hammer acceleration measured on a neighboring note on a modern piano shows some differences that might be due to distinct compression behavior of leather and felt, respectively. The comparison between measured and simulated string velocity of the D3 note played on the historic piano also shows interesting features that are likely attributable to the specificity of the Viennese action, where the hammer slips along the string before leaving it. This is known to produce a softer sound than modern pianos.

ACKNOWLEDGMENTS

This project was supported by a Lise-Meitner-Fellowship of the Austrian Science Fund (FWF; Project number M 1653-N30). The author wishes to thank Alex Mayer (University of Music and Performing Arts Vienna), Caroline Haas and Michael Kirchweger (Technical Museum Vienna), and Gert Hecher (Das Klavier-Atelier, Vienna) for their valuable help in the measurements. The simulations presented in this paper were carried out using the Plateforme Fédérative pour la Recherche en Informatique et Mathématiques (PLAFRIM) experimental platform, being developed under the Inria PlaFRIM development action with support from Institut Polytechnique de Bordeaux, Laboratoire Bordelais de Recherche en Informatique, and Institut de Mathématiques de Bordeaux and other entities: Conseil Régional d'Aquitaine, Université de Bordeaux, and Centre National de la Recherche Scientifique (and Agence Nationale de la Recherche) in accordance with the programme d'investissements d'avenir (see http://www.plafrim.fr/). The author is indebted to Juliette Chabassier and Marc Duruflé for their assistance in using the PlaFRIM environment.

APPENDIX

1. Wave analysis

For $x_s < x_H$, the pulses generated by the hammer reach the sensor at the successive instants of time

$$t_1 = (x_H - x_s)/c; \quad t_2 = (x_H + x_s)/c;$$
$$t_3 = (2L - x_H - x_s)/c; \quad t_4 = (2L - x_H + x_s)/c. \tag{A1}$$

For a hammer pulse of width τ_H, the condition for non-overlapping with the third pulse within the time interval τ_H is given by

$$t_1 + \tau_H < t_3 \Rightarrow \tau_H < 2(L - x_H)/c. \tag{A2}$$

Under this condition, the velocity signal is the sum of two waves between t_1 and $t_1 + \tau_H$. For $x_s > x_H$ and $L - x_s < x_H$ (sensor close to the bridge), we have

$$t_1 = (x_s - x_H)/c; \quad t_2 = (2L - x_H - x_s)/c;$$
$$t_3 = (x_H + x_s)/c; \quad t_4 = (2L + x_H - x_s)/c. \tag{A3}$$

The subsequent arrival times are such that $t_{i+4} = t_i + 2L/c$. The condition of non-overlapping with the fifth pulse between t_1 and τ_H then becomes

$$t_1 + \tau_H < t_5 \Rightarrow \tau_H < 2L/c = T_1. \tag{A4}$$

Under this condition, the hammer force can be reconstructed with the velocity represented by four waves. Finally, the condition of non-overlapping with the ninth pulse within the interval τ_H is

$$t_1 + \tau_H < t_9 \Rightarrow \tau_H < 4L/c = 2T_1. \tag{A5}$$

For $T_1 < \tau_H < 2T_1$, the force can then be reconstructed with the velocity signal represented by eight waves.

2. Reconstruction filter

The transfer function between string velocity and hammer force for a lossless nondispersive struck string expressed in Eq. (6) can be conveniently obtained with the help of the dual delay-line model shown in Fig. 16, adapted from the plucked string model with pickup by Karjalainen *et al.*[13] The upper delay line accounts for the wave propagation in the direction from agraffe (A1) to bridge (B1), through hammer (H1) and sensor (S1) positions. The lower delay line accounts for the propagation from bridge (B2) to agraffe (A2). The hammer force F_H gives rise to two pulses F_{H1} and F_{H2} at position x_H, and the string velocity at position x_s is the sum of the contributions V_{s1} and V_{s2} from both lines. In the case $x_H < x_s$, the delays (in samples) between the various points are

$$n_H = x_H f_e/c; \quad n_s - n_H = (x_s - x_H) f_e/c;$$
$$n_L - n_s = (L - x_s) f_e/c. \tag{A6}$$

R_a and R_b are the reflection coefficients at agraffe and bridge, respectively. On the right-hand side of the lines, we can write

$$V_s = V_{s1} + V_{s2} = V_{s1}[1 + R_b\, z^{-2(n_L - n_s)}]. \tag{A7}$$

Denoting V_{H1} the string velocity at the hammer position traveling to the right, we can write at the sensor position

$$V_{s1} = V_{H1}\, z^{-(n_s - n_H)} + R_a R_b\, z^{-2n_L}\, V_{s1}. \tag{A8}$$

Finally, at the hammer position, we can write

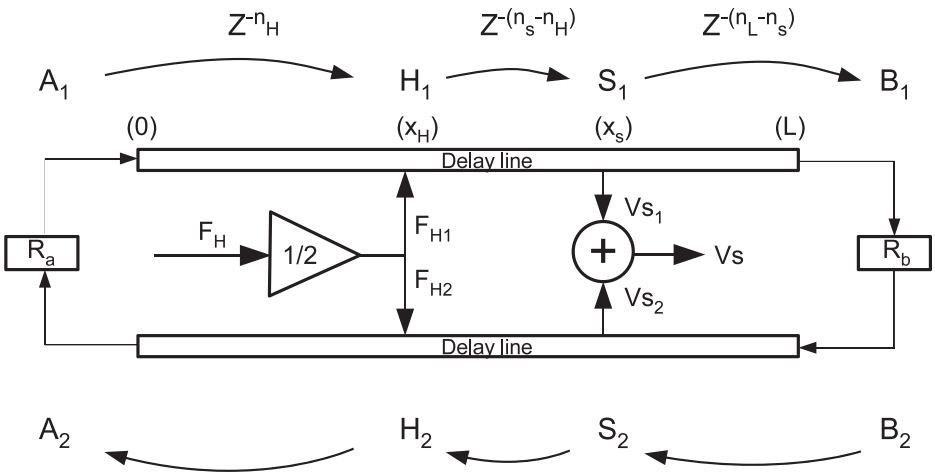

FIG. 16. Dual delay-line model for a struck string (adapted from Karjalainen *et al.*, Ref. 13). Case $x_H < x_s$.

$$V_{H1} = \frac{1}{2}\frac{F_H}{Z_c}\left[1 + R_a\, z^{-2n_H}\right]. \tag{A9}$$

From Eqs. (A7)–(A9), we get

$$H_{VF} = \frac{V_s}{F_H} = \frac{1}{2Z_c}\frac{z^{-n_1}\left[1 + R_a\, z^{-m_1}\right]\left[1 + R_b\, z^{-m_2}\right]}{1 - R_a R_b\, z^{-m_3}}, \tag{A10}$$

with $n_1 = n_s - n_H$, $m_1 = 2n_H$, $m_2 = 2(n_L - n_s)$ and $m_3 = 2n_L$. For perfect reflecting ends, we have $R_a = R_b = -1$. For dissipative ends, we can write $R_a = -g_1$ and $R_b = -g_2$, with $|g_1|, |g_2| < 1$.

[1]X. Boutillon, "Model for piano hammers: Experimental determination and digital simulation," J. Acoust. Soc. Am. **83**(2), 746–754 (1988).
[2]D. E. Hall and A. Askenfelt, "Piano string excitation V: Spectra for real hammers and strings," J. Acoust. Soc. Am. **83**(4), 1627–1638 (1988).
[3]S. Birkett, "Experimental investigation of the piano hammer-string interaction," J. Acoust. Soc. Am. **133**(4), 2467–2478 (2013).
[4]A. Askenfelt and E. V. Jansson, "From touch to string vibrations. II: The motion of the key and hammer," J. Acoust. Soc. Am. **90**(5), 2383–2393 (1991).
[5]N. Giordano and J. P. Winans, "Piano hammers and their force compression characteristics: Does a power law make sense?," J. Acoust. Soc. Am. **107**(4), 2248–2255 (2000).
[6]J. Chabassier and M. Duruflé, "Energy based simulation of a Timoshenko beam in non-forced rotation. Influence of the piano hammer shank flexibility on the sound," J. Sound Vib. **333**(26), 7198–7215 (2014).
[7]J. Woodhouse, R. T. Schumacher, and S. Garoff, "Reconstruction of bowing point friction force in a bowed string," J. Acoust. Soc. Am. **108**(1), 357–368 (2000).
[8]J. Chabassier, A. Chaigne, and P. Joly, "Modeling and simulation of a grand piano," J. Acoust. Soc. Am. **134**(1), 648–665 (2013).
[9]P. M. Morse, *Vibration and Sound* (Acoustical Society of America, Melville, NY, 1981), Chap. 3, pp. 61–147.
[10]A. Chaigne and A. Askenfelt, "Numerical simulations of piano strings. I. A physical model for a struck string using finite difference methods," J. Acoust. Soc. Am. **95**(2), 1112–1118 (1994).
[11]H. A. Conklin, "Design and tone in the mechanoacoustic piano. Part III. Piano strings and scale design," J. Acoust. Soc. Am. **100**, 1286–1298 (1996).
[12]J. O. Smith, *Introduction to Digital Filters with Audio Applications* (W3K Publishing, Palo Alto, CA, 2007), Chap. 3, pp. 47–81. Available at http://books.w3k.org/ (Last viewed 3/17/2016).
[13]M. Karjalainen, V. Välimäki, and T. Tolonen, "Plucked-string models: From the Karplus-Strong algorithm to digital waveguides and beyond," Comput. Music J. **22**(3), 17–32 (1998).
[14]J. S. Abel, V. Välimäki, and J. O. Smith III, "Robust, efficient design of allpass filters for dispersive string sound synthesis," IEEE Signal Proc. Lett. **17**(4), 406–409 (2010).
[15]J. S. Abel and J. O. Smith, "Robust design of very high-order allpass dispersion filters," in *Proceedings of the 9th Int. Conference on Digital Audio Effects*, Montreal (2006), pp. 13–18.
[16]J.-P. Thiran, "Recursive digital filters with maximally flat group delay," IEEE Trans. Circuit Theory **18**(6), 659–664 (1971).
[17]J. Chabassier, A. Chaigne, and P. Joly, "Time domain simulation of a piano. Part 1: Model description," ESAIM: Math. Modell. Numer. Anal. **48**(5), 1241–1278 (2014).
[18]P. M. Morse and K. U. Ingard, *Theoretical Acoustics* (McGraw-Hill, New York, 1968), Chap. 14, 857–860.
[19]H. Suzuki and I. Nakamura, "Acoustics of pianos," Appl. Acoust. **30**, 147–205 (1990).
[20]A. Stulov, "Experimental and computational studies of piano hammers," Acta Acust. Acust. **91**(6), 1086–1097 (2005).
[21]J. O. Smith III, "Physical modeling using digital waveguides," Comput. Music J. **16**(1), 74–87 (1992).
[22]G. V. Anand, "Large amplitude damped free vibration of a stretched string," J. Acoust. Soc. Am. **45**(5), 1089–1096 (1969).
[23]M. Latcham, "The check in some early pianos and the development of piano technique around the turn of the 18th century," Early Music **21**(1), 29–42 (1993).